

Supporting Information for

Discovery of a Self-healing Catalyst for the Hydrolytic Dehydrogenation of Ammonia Borane

*F. Pelin Kinik,¹ Tu N. Nguyen,¹ Emad Oveisi,² Bardiya Valizadeh,¹ Fatmah Mish Ebrahim,¹ Andrzej Gładysiak,¹ Mounir Mensi³ and Kyriakos C. Stylianou^{*1}*

1 Laboratory for Molecular Simulation (LSMO), Institute of Chemical Sciences and Engineering, École Polytechnique Fédérale de Lausanne (EPFL Valais), Rue de l'Industrie 17, 1951 Sion, Switzerland.

2 Interdisciplinary Center for Electron Microscopy, École Polytechnique Fédérale de Lausanne (EPFL), 1015 Lausanne, Switzerland.

3. Institute of Chemical Sciences and Engineering, École Polytechnique Fédérale de Lausanne (EPFL Valais), Rue de l'Industrie 17, 1951 Sion, Switzerland.

*e-mail: kyriakos.stylianou@epfl.ch

EXPERIMENTAL SECTION

Material characterization: Powder X-ray diffraction (PXRD) data on all samples were collected on a Bruker D8 Advance diffractometer at ambient temperature using monochromated Cu K α radiation ($\lambda = 1.5418 \text{ \AA}$), with a 2θ step of 0.02° and a 2θ range of ~ 2 to 70° . Simulated PXRD patterns were generated from the corresponding crystal structures using Mercury 3.0. The Fourier-Transform Infrared (FTIR) measurements were performed with the Spectrum Two FTIR spectrometer (Perkin Elmer) in the transmittance mode from 400 to 4000 cm^{-1} . The N₂ adsorption isotherm measurements were performed at 77 K by using BELSORP Mini (BEL Japan, Inc.). Prior to measurements, samples were activated at 120 °C for 12 h under vacuum. A part of the nitrogen adsorption isotherm in the P/P_0 range 0.06–0.25 was fitted to the Branuner-Emmett-Teller (BET) equation to estimate the surface areas of the samples. The morphologies of the Cu-bpy-Y MOFs

and **SION-X** were investigated by scanning electron microscopy (SEM) on the FEI Teneo SEM instrument. For SEM measurements, all samples were deposited on a carbon tape and coated with a 7-nm thick Iridium layer prior imaging. Conventional transmission electron microscopy (TEM) images and selected area electron diffraction patterns were collected on the FEI Tecnai Spirit instrument at 120 kV acceleration voltage. High-angle annular dark-field images were collected on a FEI Titan Themis TEM operated at 200 kV in scanning mode. A PerkinElmer Thermogravimetry Analyzer (TGA) was used to determine the decomposition temperature of the samples. All measurements were performed under air flow up to 600 °C. Inductively coupled plasma optical emission spectrometry (ICP-OES) measurements were performed using a NexIon 350 (Perkin Elmer) spectrometer. X-ray photoelectron spectroscopy (XPS) experiments were performed using PHI 5000 Versaprobe-II instrument from Physical Electronics. Samples were deposited on an insulating double sided, vacuum compatible, tape, and charge neutralization was applied during the XPS measurements. The binding energy scale was then corrected with the C-C bound of the C1s photoelectron peak located at 284.6 eV. Peak fitting of the Cu 2p_{3/2} photoelectron peak, along with the kinetic energy of the Cu L₃M₄₅M₄₅ peak, were used to evaluate the chemical state of copper.¹

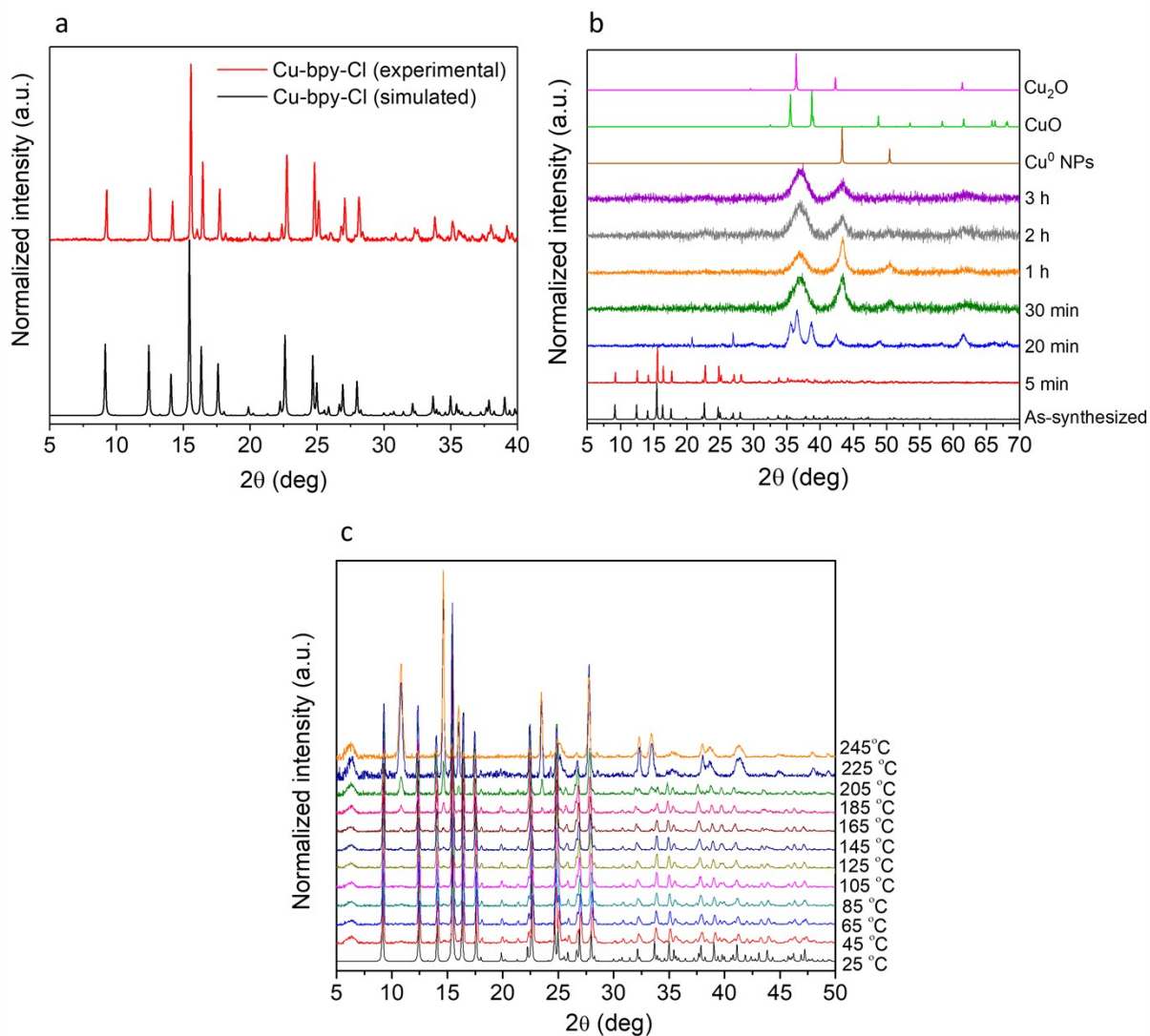


Figure S1. **a)** Comparison of the simulated PXRD pattern of Cu-bpy-Cl with the experimental one. **b)** PXRD patterns of the Cu-bpy-Cl at different times of AB hydrolysis, showing the reduction of Cu^{I} in MOF structure and formation of Cu NPs. The diffraction patterns of CuO and Cu_2O are also given in the figure to demonstrate the surface oxidation of metallic copper. **c)** Variable temperature PXRD pattern of Cu-bpy-Cl up to 245 $^\circ\text{C}$.

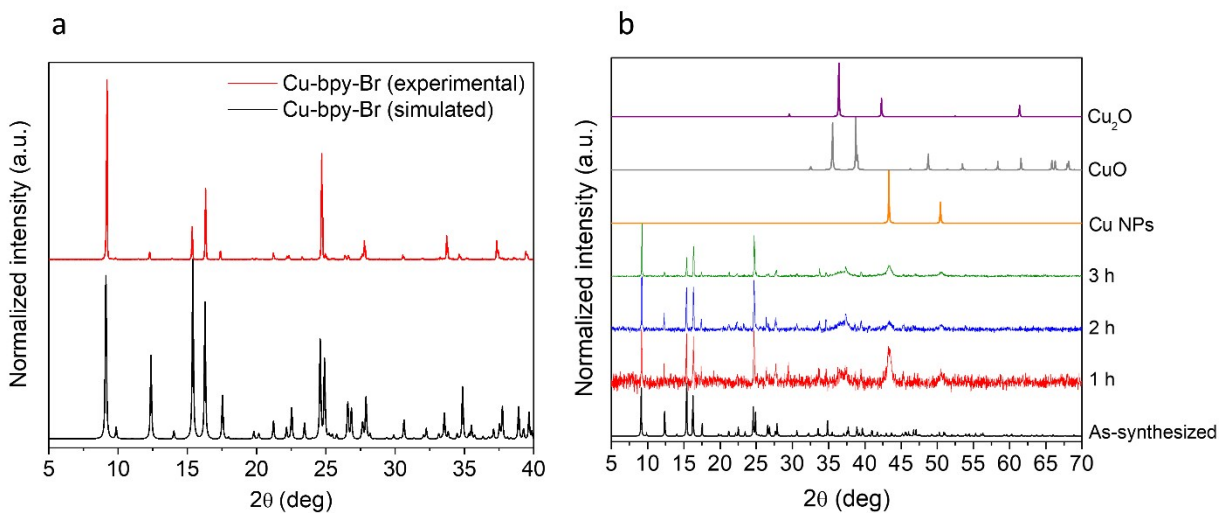


Figure S2. a) Comparison of the simulated PXRD pattern of Cu-bpy-Br with the experimental one. **b)** PXRD patterns of the Cu-bpy-Br at different reaction times of AB hydrolysis.

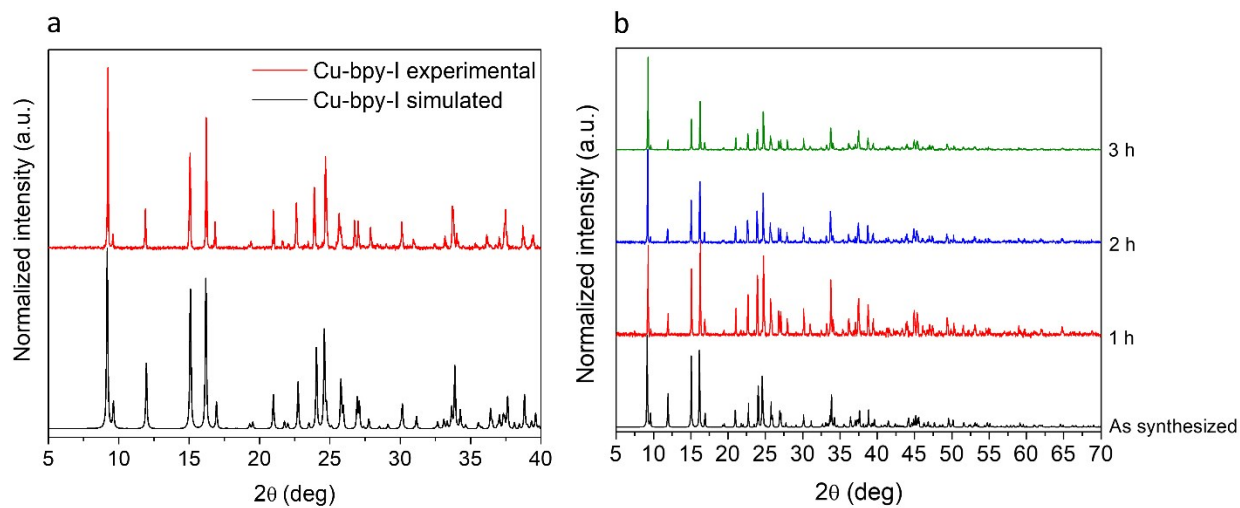


Figure S3. a) Comparison of the simulated PXRD pattern of Cu-bpy-I with the experimental one. **b)** PXRD patterns of the Cu-bpy-I at different reaction times of AB hydrolysis.

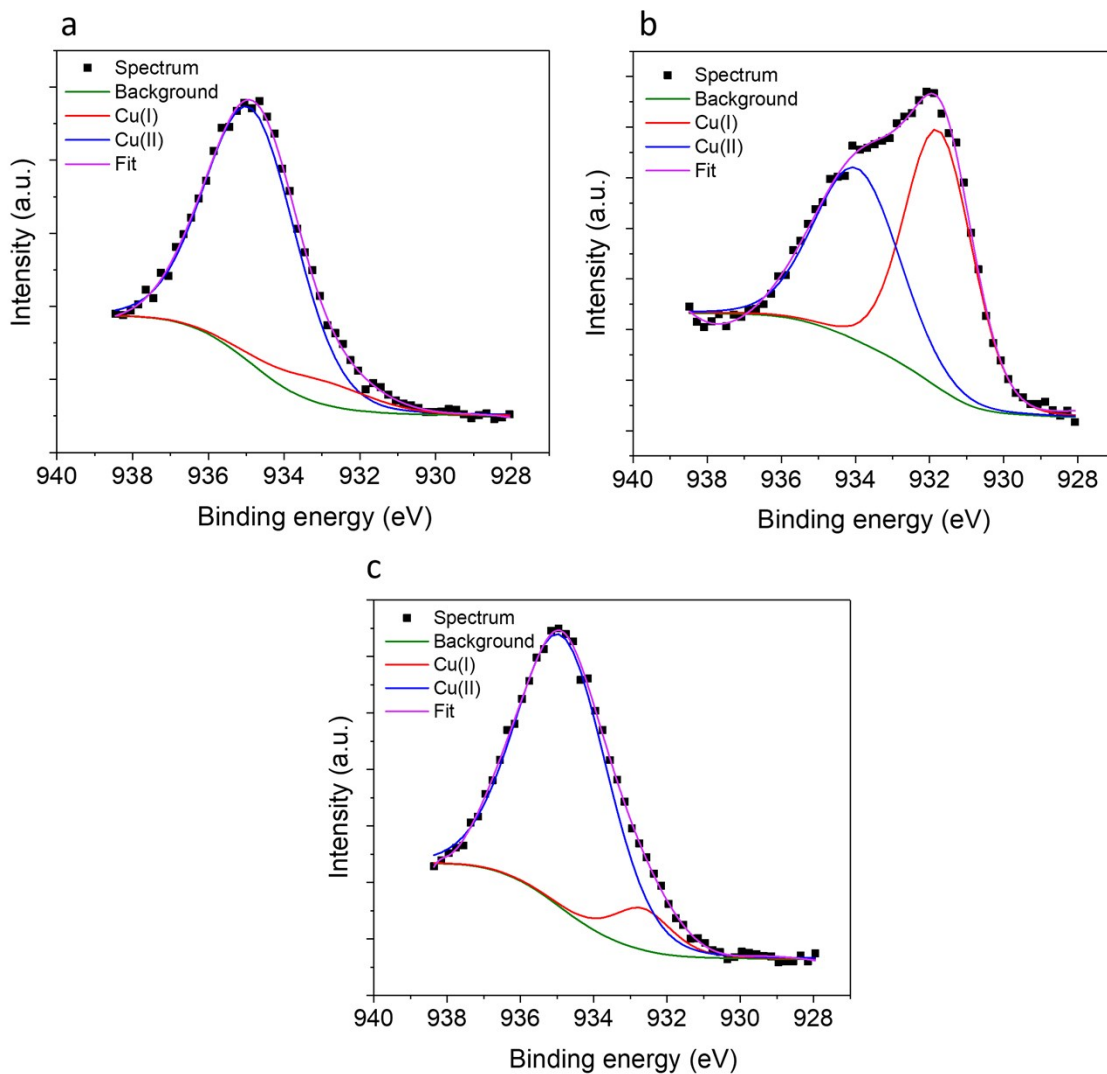


Figure S4. Cu 2p XPS spectra of **a)** as-synthesized **SION-X**, **b)** Cu NPs derived from **SION-X** during AB hydrolysis and **c)** Cu-bpy-Cl collected after AB hydrolysis. Since all samples are exposed to air, Cu⁰ NPs were oxidized and formed Cu₂O and Cu^{II}O

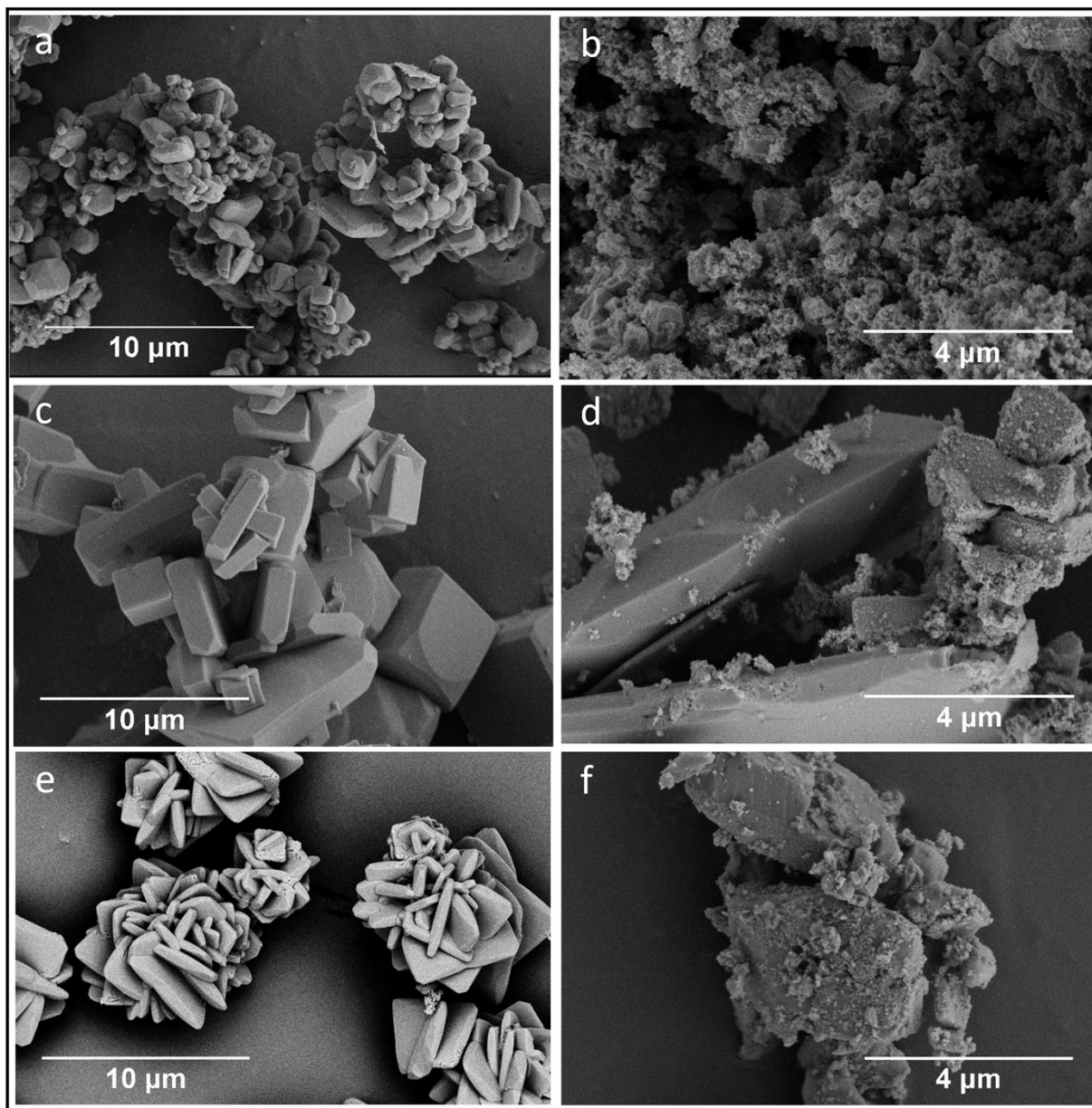


Figure S5. SEM images of Cu-bpy-Y before (Y = **a**) Cl , **c**) Br, and **e**) I) and after (X = **b**) Cl, **d**) Br, and **f**) I) after 3 hours of AB hydrolysis.

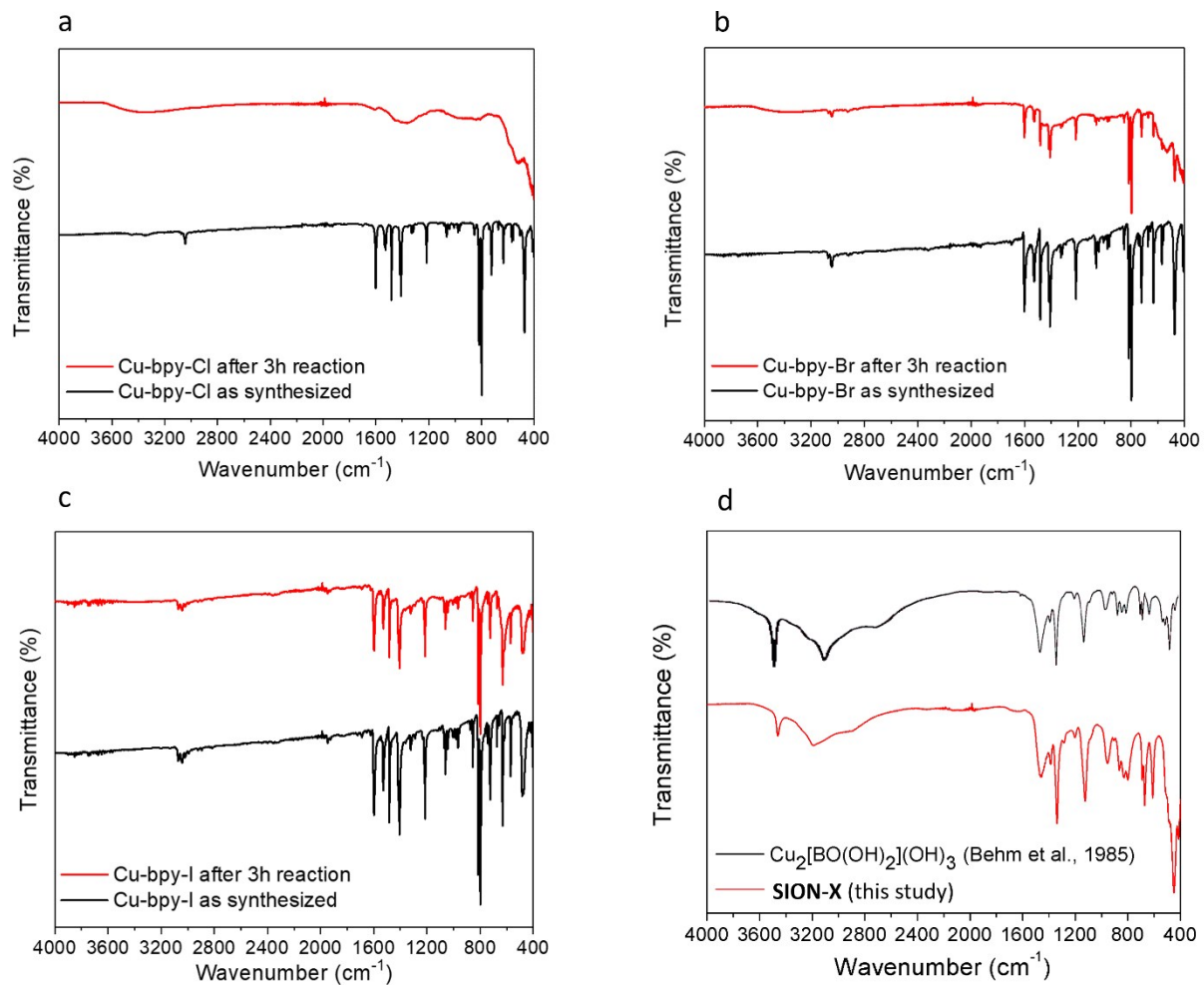


Figure S6. FTIR spectra of **a)** Cu-bpy-Cl, **b)** Cu-bpy-Br, **c)** Cu-bpy-I before (black) and after (red) AB hydrolysis and **d)** SION-X in comparison with the FTIR spectrum of Cu₂[BO(OH)₂](OH)₃ synthesized by Behm *et al.*²

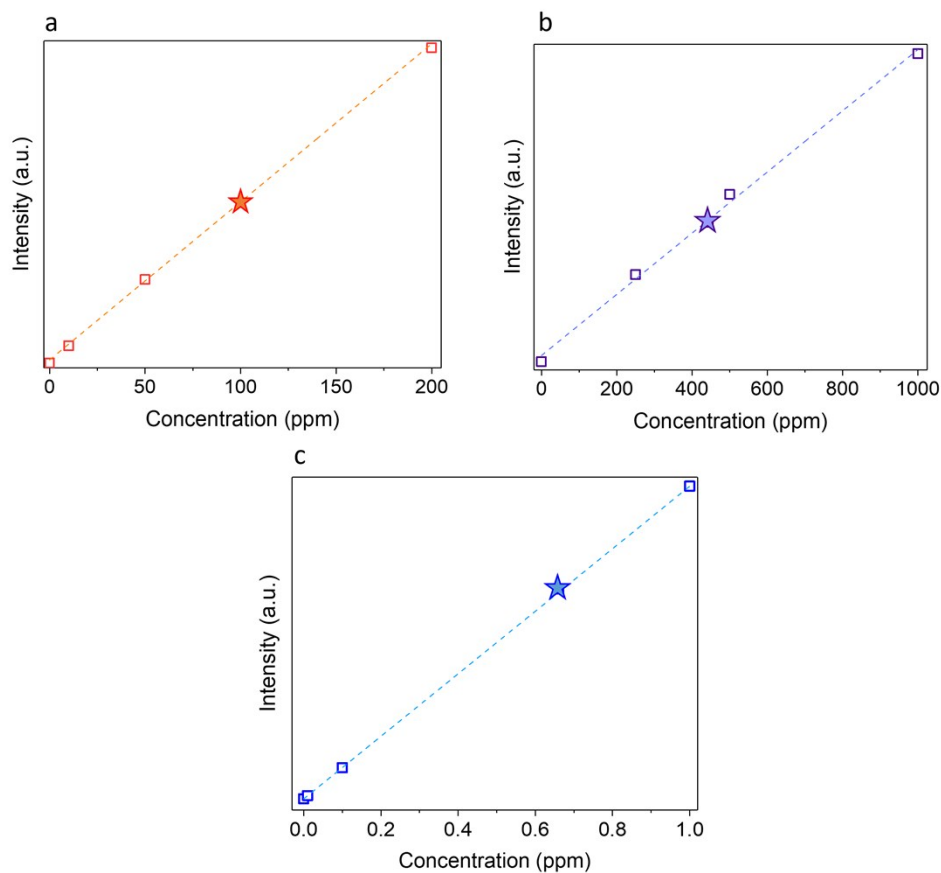


Figure S7. Concentrations of **a)** copper and **b)** boron determined by ICP-OES measurements by analyzing **SION-X** digested in acid. For Cu analysis, a solution was prepared by dissolving 1.88 mg **SION-X** in dilute HNO_3 , giving a concentration of 100 ppm. For B analysis, a solution was prepared by dissolving 55.24 mg **SION-X** in a mixture of concentrated HNO_3 and Millipore water, giving a concentration of 500 ppm. **c)** Concentration of copper in the supernatant after **SION-X** was regenerated, showing that negligible amount of Cu is lost into the solution.

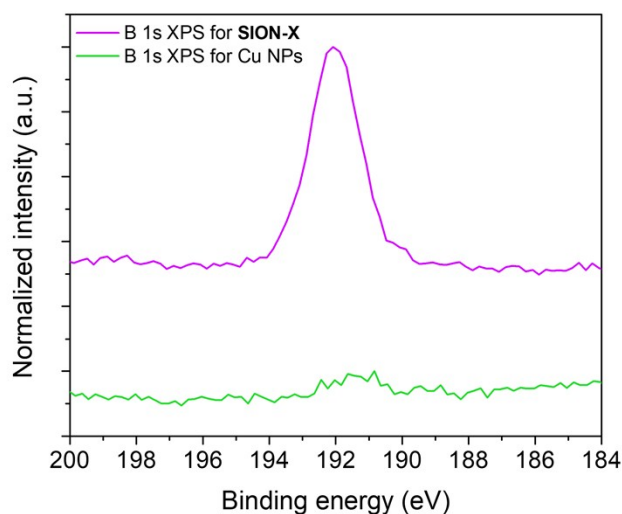


Figure S8. B 1s XPS peaks for as synthesized SION-X (purple) and Cu NPs derived from SION-X during AB hydrolysis (green).

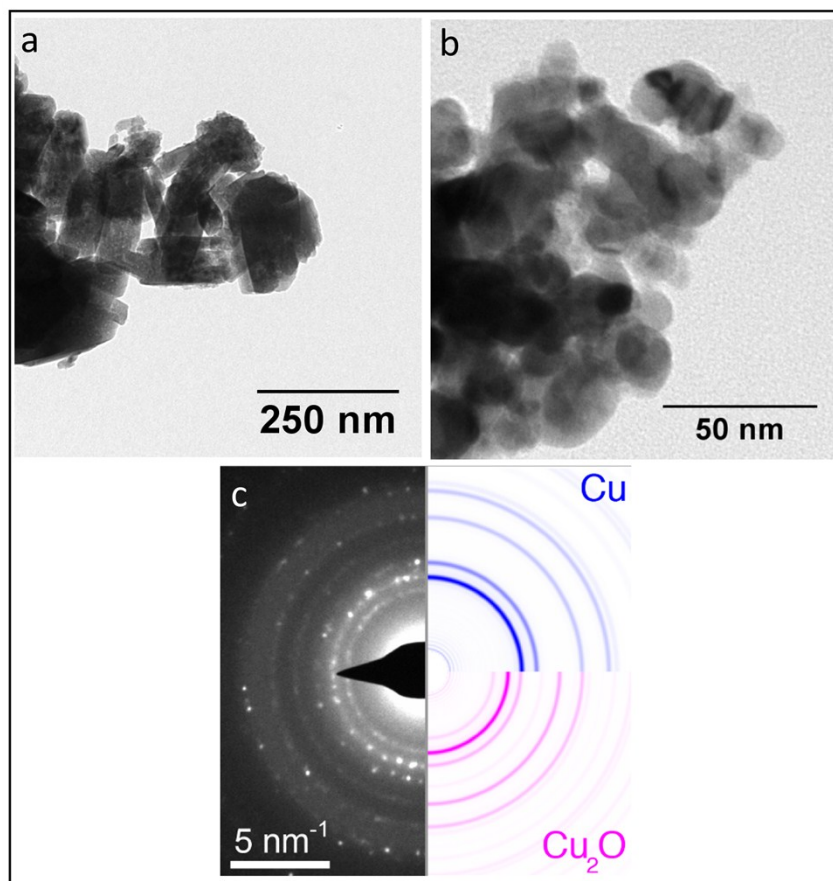


Figure S9. **a)** Bright-field TEM image of SION-X, showing that SION-X is composed of crystals with cuboid shapes, **b)** Bright-field TEM image of SION-X after AB hydrolysis, **c)** selected area electron diffraction pattern of SION-X sample that was obtained after AB hydrolysis using SION-X, showing that the final material is composed of Cu⁰ and Cu₂O NPs. Simulated electron

diffraction patterns (ring sampling diffraction planes) of Cu and Cu₂O are shown to the right of c.

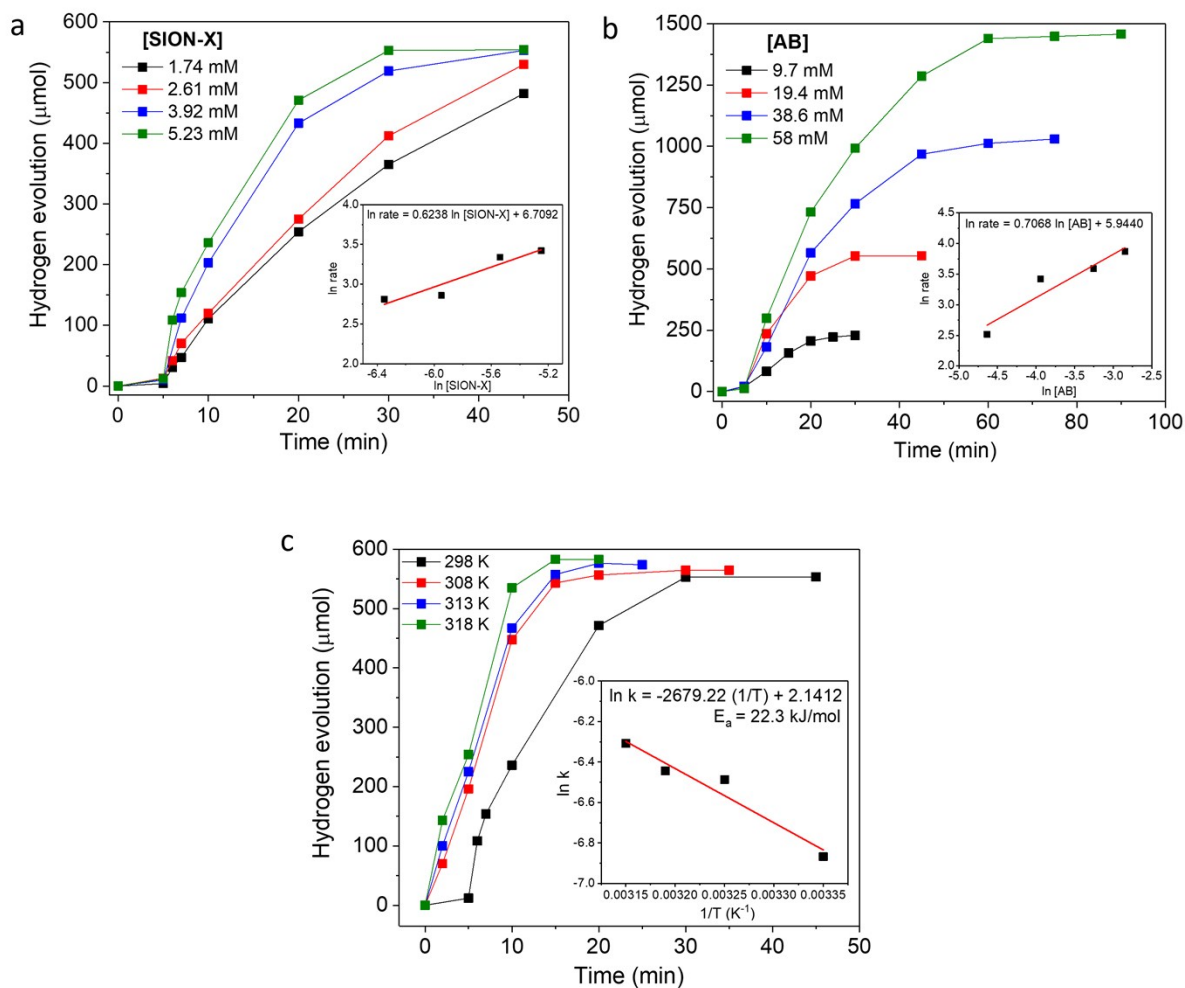


Figure S10. Hydrogen evolution from AB in aqueous solution (10 ml) at 298 K containing **a)** fixed amount of AB (0.1944 mmol) at various **SION-X** amounts (inset: logarithmic plots of hydrogen evolution rate vs catalyst concentration) and **b)** fixed amount of catalyst (0.052 mmol) at various AB concentrations (inset: logarithmic plots of hydrogen evolution rate vs AB concentration); **c)** Hydrogen evolution rate of AB hydrolysis catalyzed by **SION-X** catalyst at different temperatures containing fixed amount of AB and **SION-X** (inset: Arrhenius plot ($\ln k$ vs $1/T$)).

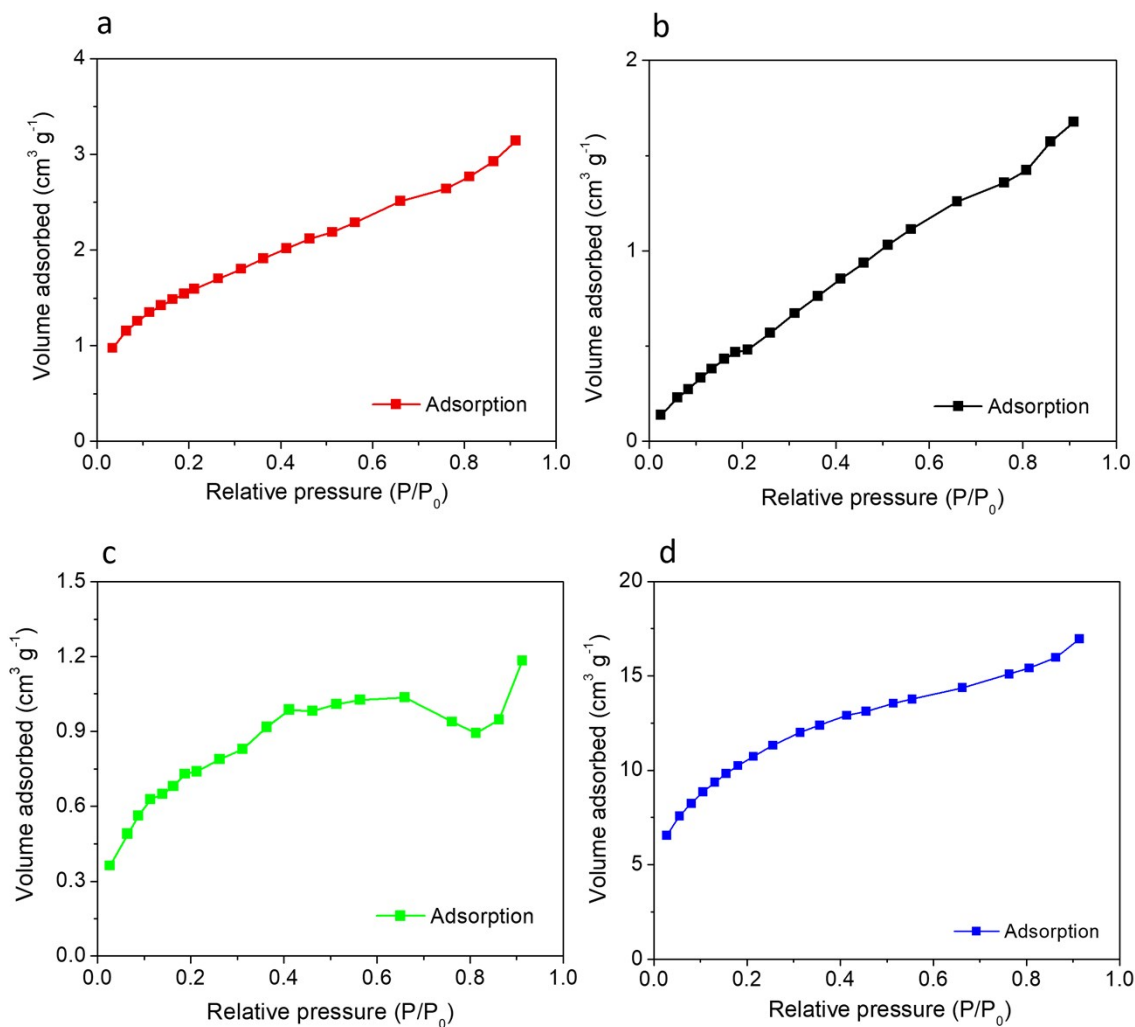


Figure S11. Nitrogen adsorption isotherms of **a)** Cu-bpy-Cl, **b)** Cu-bpy-Br, **c)** Cu-bpy-I and **d)** SION-X. Cu-bpy-Y MOFs are non-porous while SION-X has a BET surface area of 39.24 m² g⁻¹.

1.

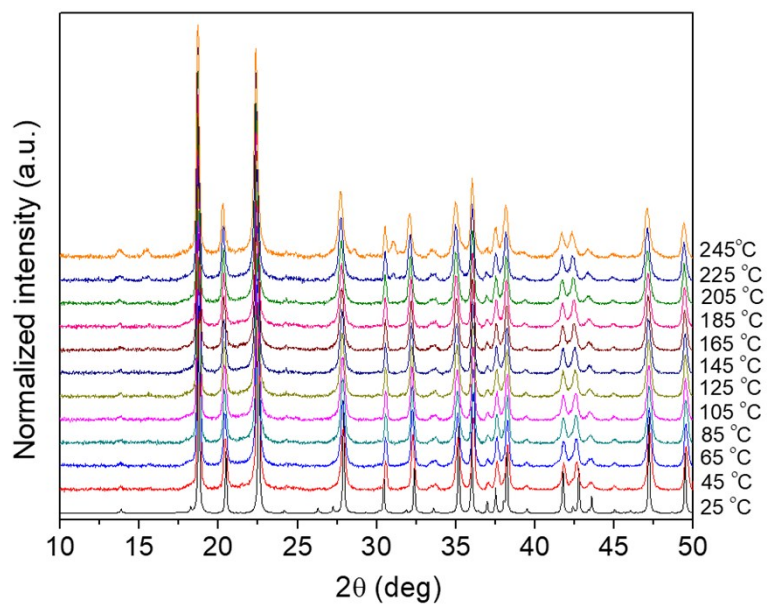


Figure S12. Variable temperature PXRD pattern of **SION-X** up to 245 °C showing the remarkable stability of the structure.

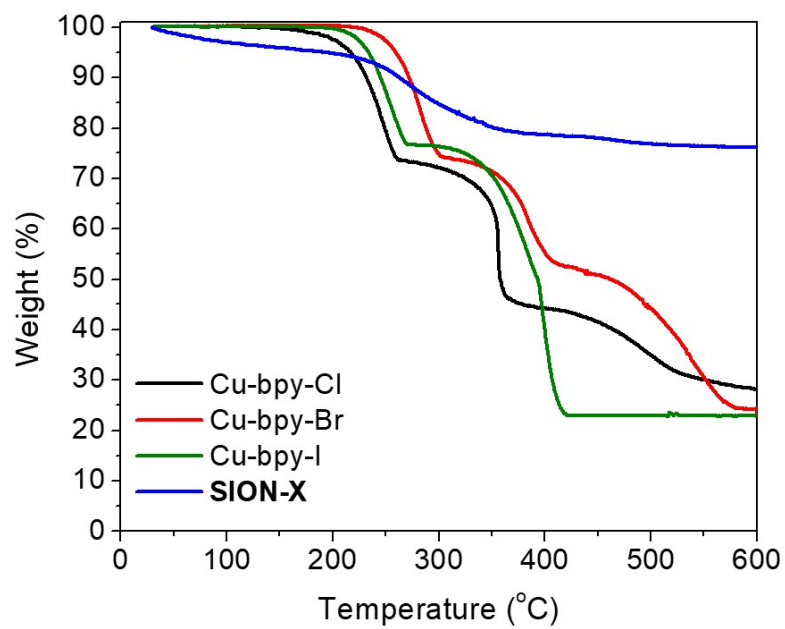


Figure S13. Thermal gravimetric analysis of Cu-bpy-Cl (black), Cu-bpy-Br (red), Cu-bpy-I (green) and **SION-X** (blue). Cu-bpy-Y MOFs are thermally stable up to 217, 256 and 232 °C, respectively, while **SION-X** is thermally stable up to 245 °C.

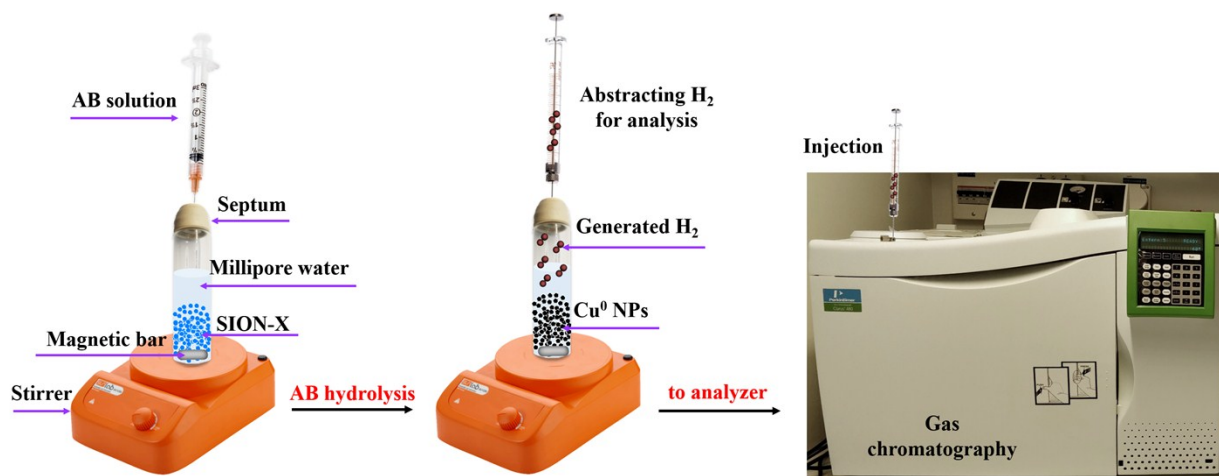


Figure S14. The catalytic setup for AB hydrolysis.

Table S1. Catalytic activity of some copper-based catalysts used for AB hydrolysis

Catalyst	E _a (kJ mol ⁻¹)	TOF (min ⁻¹)	Retained activity at reuse (%) ^a	Ref.
Cu/zeolite	52	0.78	53% at 5 th use	3
Cu _{0.2} @Co _{0.8} /rGO	51.3	8.36	78% at 3 th use	4
p(AMPS)-Cu	48.8	0.72	93% at 4 th use	5
Annealed-RGO-Cu ₇₅ Pd ₂₅	45.0	29.90 ^b	70% at 3 rd run	6
Cu(OH) ₂ @Co ₂ CO ₃ (OH) ₂ /CF	44.3	39.72	80% at 7 th run	7
Cu _{0.33} Fe _{0.67}	43.2	-	40% at 10 th use	8
Cu _{0.2} Co _{0.8} /HPC	41.7	-	40% at 4 th use	9
CoNi/RGO	39.9	19.54	68% at 5 th run	10
Cu _{0.3} @Fe _{0.1} Co _{0.6}	38.7	10.50	40% at 4 th use	11
Cu/RGO	38.2	3.61	>95% at 4 th use	12
Cu _{0.2} Ni _{0.8} /MCM-41	38	10	30% at 10 th use	13
Cu@CoNi core-shell	36	-	35% at 5 th use	14
Cu@SiO ₂	36	3.24	90% at 10 th use	15
Cu _{0.4} @Fe _{0.1} Ni _{0.5}	32.9	-	90% at 5 th use	16
CuCo ₂ O ₄ NPs	32.0	10.90	67% at 8 th use	17
Cu@FeCoNi/graphene	31.8	20.93	43% at 5 th run	18
RuCu/graphene	30.4	15.90	65% at 5 th use	19
NiCu nanorods@C nanofibers	28.9	-	100% at 6 th use	20
Cu _{0.5} Co _{0.5} @SiO ₂	24	-	>90% at 10 th use	21
Cu/h-BN	23.8	0.32	40% at 5 th use	22
SION-X	22.3	1.85^c (0.97)^d	92% at 10th use	This work
Cu _{0.81} @Mo _{0.09} Co _{0.10}	22.2	49.61	42% at 4 th run	23
Cu NPs	-	0.06	-	24
Cu ₂ O NPs	-	0.18	-	
Cu@Cu ₂ O	-	0.25	90% at 9 th use	
CuO	-	0.16	30% at 2 nd use	25
Cu NPs@TiO ₂	-	0.18	-	26
CuCl ₂	-	0.23	-	27
Cu/γ-Al ₂ O ₃	-	0.27	-	28

a. The activities are given based on the comparison with the activity at 1st cycle.

b. Initial activation energy.

- c. TOF at 50% conversion.
- d. TOF based on Cu.

Table S2. Concentrations of copper and boron obtained by digesting **SION-X** in acidic solution

	Cu in SION-X (calculated)	Cu in SION-X (found)	B in SION-X (calculated)	B in SION-X (found)
Concentration (ppm)	100	100.8	500	443.6

References

1. M. C. Biesinger, L. W. Lau, A. R. Gerson, R. S. C. Smart, *Appl. Surf. Sci.*, 2010, **257**, 887.
2. H. Behm, C. Baerlocher, *Acta Crystallogr. Sect. C: Cryst. Struct. Commun.*, 1985, **41**, 5.
3. M. Zahmakıran, F. Durap, S. Özkar, *Int. J. Hydrogen Energy*, 2010, **35**, 187.
4. Y. Du, N. Cao, L. Yang, W. Luo, G. Cheng, *New J. Chem.*, 2013, **37**, 3035.
5. O. Ozay, E. Inger, N. Aktas, N. Sahiner, *Int. J. Hydrogen Energy*, 2011, **36**, 8209.
6. K. Güngörmez, Ö. Metin, *Appl. Catal., A*, 2015, **494**, 22.
7. J. Wang, X. Ma, W. Yang, X. Sun, J. Liu, *Nanotechnology*, 2016, **28**, 045606.
8. Z.-H. Lu, J. Li, A. Zhu, Q. Yao, W. Huang, R. Zhou, R. Zhou, X. Chen, *Int. J. Hydrogen Energy*, 2013, **38**, 5330.
9. H. Wang, L. Zhou, M. Han, Z. Tao, F. Cheng, J. Chen, *J. Alloys Compd.*, 2015, **651**, 382.
10. Y. Yang, F. Zhang, H. Wang, Q. Yao, X. Chen, Z.-H. Lu, *J. Nanomater.*, 2014, **2014**, 3.
11. F. Qiu, Y. Dai, L. Li, C. Xu, Y. Huang, C. Chen, Y. Wang, L. Jiao, H. Yuan, *Int. J. Hydrogen Energy*, 2014, **39**, 436.
12. Y. Yang, Z.-H. Lu, Y. Hu, Z. Zhang, W. Shi, X. Chen, T. Wang, *RSC Adv.*, 2014, **4**, 13749.
13. Z.-H. Lu, J. Li, G. Feng, Q. Yao, F. Zhang, R. Zhou, D. Tao, X. Chen, Z. Yu, *Int. J. Hydrogen Energy*, 2014, **39**, 13389.
14. H. Zhang, X. Wang, C. Chen, C. An, Y. Xu, Y. Huang, Q. Zhang, Y. Wang, L. Jiao, H. Yuan, *Int. J. Hydrogen Energy*, 2015, **40**, 12253.
15. Q. Yao, Z.-H. Lu, Z. Zhang, X. Chen, Y. Lan, *Sci. Rep.*, 2014, **4**, 7597.
16. H.-L. Wang, J.-M. Yan, Z.-L. Wang, Q. Jiang, *Int. J. Hydrogen Energy*, 2012, **37**, 10229.
17. Q. Liu, S. Zhang, J. Liao, K. Feng, Y. Zheng, B. G. Pollet, H. Li, *J. Power Sources*, 2017, **355**, 191.
18. X. Meng, S. Li, B. Xia, L. Yang, N. Cao, J. Su, M. He, W. Luo, G. Cheng, *RSC Adv.*, 2014, **4**, 32817.
19. L. Wen, J. Su, X. Wu, P. Cai, W. Luo, G. Cheng, *Int. J. Hydrogen Energy*, 2014, **39**, 17129.

20. A. Yousef, N. A. Barakat, M. El-Newehy, H. Y. Kim, *Int. J. Hydrogen Energy*, 2012, **37**, 17715.
21. Q. Yao, Z.-H. Lu, Y. Wang, X. Chen, G. Feng, *J. Phys. Chem. C*, 2015, **119**, 14167.
22. X. Qiu, X. Wu, Y. Wu, Q. Liu, C. Huang, *RSC Adv.*, 2016, **6**, 106211.
23. C. Wang, H. Wang, Z. Wang, X. Li, Y. Chi, M. Wang, D. Gao, Z. Zhao, *Int. J. Hydrogen Energy*, 2018, **43**, 7347.
24. S. B. Kalidindi, U. Sanyal, B. R. Jagirdar, *Phys. Chem. Chem. Phys.*, 2008, **10**, 5870.
25. Y. Yamada, K. Yano, Q. Xu, S. Fukuzumi, *J. Phys. Chem. C*, 2010, **114**, 16456.
26. M. Kaya, M. Zahmakiran, S. Özkar, M. R. Volkan, *ACS Appl. Mater. Interfaces*, 2012, **4**, 3866.
27. S. B. Kalidindi, M. Indirani, B. R. Jagirdar, *Inorg. Chem.*, 2008, **47**, 7424.
28. Q. Xu, M. Chandra, *J. Power Sources*, 2006, **163**, 364.